# Electron-phonon effects in copper. I. Electron scattering rate and mass enhancement

F. S. Khan and P. B. Allen
*Department of Physics, State University of New York at Stony Brook, Stony Brook, New York 11794*

W. H. Butler
*Oak Ridge National Laboratory, Oak Ridge, Tennessee 37830*

F. J. Pinski
*Department of Physics, University of Cincinnati, Cincinnati, Ohio 45221*
(Received 4 March 1982)

Phonon-limited quasiparticle-mass enhancement $\lambda_{\vec{k}}$ and low-temperature lifetimes $1/\tau_{\vec{k}}=c_{\vec{k}}T^3$ are calculated for Cu. Experimental phonons, Korringa-Kohn-Rostocker wave functions and the rigid-muffin-tin (RMT) model have been used. The results are compared with calculations of other groups and with experiment. It is found that the experiment of Doezema and Koch (DK) was not performed at a low enough temperature ($T$) to give the correct limiting value of $c_{\vec{k}}$. The results at higher $T$ match well the data of DK and the calculation of Schmidt and Mann, but do not agree closely with the calculations of Nowak and Das. In contradiction to an earlier suggestion, the RMT model seems to work well at small momentum transfers.

## I. INTRODUCTION

In a metal, the electron-phonon interaction gives rise to a complex, frequency-dependent electronic self-energy. The electronic mass enhancement $\lambda_{\vec{k}}$ is obtained from the real part of the self-energy and the scattering rate $1/\tau_{\vec{k}}$ from the imaginary part.[1] Calculations of $\lambda_{\vec{k}}$ and $1/\tau_{\vec{k}}$ for Cu have been performed before by a number of authors[2–4] and compared with experiment.[5,6] Thus Cu serves as an important test case. As part of a project to evaluate electron-phonon effects in transition metals,[7,8] we therefore tested our procedures on Cu. The results are published here for the following reasons:

(1) We believe that we have calculated $1/\tau_{\vec{k}}$ more carefully than ever before and have a more detailed comparison with experimental data of Doezema and Koch[6] (DK).

(2) Our procedures for calculating $1/\tau_{\vec{k}}$ were only briefly outlined in a short paper on Pd,[9] and the procedures for calculating $\lambda_{\vec{k}}$ were omitted entirely from a paper on Nb and Cu.[10] This paper describes the procedures used in those earlier calculations.

(3) The following paper[11] presents calculations of $\rho$, $W$, and $R_H$ (electrical and thermal resistivity and Hall coefficient) for Cu. The present paper serves as an introduction and as a reference point for the subsequent paper.

Section II of this paper contains a description of our method of calculating $\lambda_{\vec{k}}$ and a comparison with the calculations of other groups and experiment. Section III contains a description of our methods and results for $1/\tau_{\vec{k}}T^3$ for small $T$. We make a detailed comparison with the experiment of DK (Ref. 6) and the theoretical work of Nowak (Ref. 2) and Schmidt and Mann (Ref. 4). In Sec. IV we present our conclusions. The Appendix contains a description of how the potential used in our calculations is constructed.

## II. MASS ENHANCEMENT

The phonon-limited electronic mass enhancement $\lambda_{\vec{k}}$ is given by the expression [Eq. (5.61) of Ref. 1]

$$\lambda_{\vec{k}}=\frac{2}{N}\sum_{\vec{k}'}\sum_{\nu}|g^{\nu}_{\vec{k},\vec{k}'}|^2\omega^{\nu\,-1}_{\vec{k}-\vec{k}'}\delta(\epsilon_{\vec{k}'})\,, \tag{1}$$

$$g^{\nu}_{\vec{k},\vec{k}'}=\hat{\epsilon}^{\nu}_{\vec{k}-\vec{k}'}\cdot\langle\psi_{\vec{k}}|\vec{\nabla}V|\psi_{\vec{k}'}\rangle\left[\frac{1}{2M\omega^{\nu}_{\vec{k}-\vec{k}'}}\right]^{1/2}. \tag{2}$$

The notation is consistent with Refs. 7 and 8, i.e., $\hat{\epsilon}^{\nu}_{\vec{Q}}$ is the polarization vector of a phonon with wave vector $\vec{Q}$ and frequency $\omega^{\nu}_{\vec{Q}}$ belonging to the branch $\nu$, and $M$ is ionic mass. The calculation of $\lambda_{\vec{k}}$ needs the following ingredients[7,8]:

(i) A mesh of points on the Fermi surface (FS); specifically, we use 492 points in $\frac{1}{48}$th of the Bril-

 

louin zone (BZ). At each of these points, Korringa-Kohn-Rostoker (KKR) wave functions $\psi_{\vec{k}}$ are calculated using 16 spherical harmonics (maximum $l=3$).

(ii) Phonon-polarization vectors and frequencies are obtained from Born—von Kármán force constants fitted to inelastic neutron scattering data.[12]

(iii) The rigid muffin-tin (RMT) model has been used to calculate electron-phonon matrix elements $g^{\nu}_{\vec{k},\vec{k}'}$. The RMT was designed for transition metals where the electronic wave-function amplitude is small outside the muffin-tin (MT). In Cu, this is not a very good model. However, by using the freedom of choice of the MT zero, one can rescale the phase shifts without altering the band structure and thus attempt to improve the electron-phonon matrix elements.[13] Our procedure is similar to that used by Nowak[2] and is described in the Appendix.

The calculation of $\lambda_{\vec{k}}$ proceeds as follows. The $\frac{1}{48}$th of the BZ is divided into 1378 bins, and each bin is assigned three polarization vectors and frequencies corresponding to the $\vec{Q}$ vector at the center of the bin. In order to perform the FS integration in Eq. (1), $\vec{k}'$ is made to assume all the 492 values in $\frac{1}{48}$th of the BZ on the FS. The 48 cubic-point-group operations are performed on $\vec{k}'$ so that the point $\vec{k}'$ traces the whole FS. For each $\vec{k}'$ the vector $\vec{k}-\vec{k}'-\vec{K}=\vec{Q}$ is obtained, where $\vec{K}$ is the reciprocal-lattice vector which brings $\vec{k}-\vec{k}'$ into the first BZ. The point-group operation required to rotate $\vec{Q}$ into the $\frac{1}{48}$th of the BZ is determined, and the phonon frequencies and polarization vectors of the corresponding $\vec{Q}$ bin are used. The wave functions are obtained by the appropriate point-group operation and the matrix elements are calculated.

The resulting angular variation of $\lambda_{\vec{k}}$ in symmetry planes of Cu is plotted in Figs. 1 and 2 along with the previous results obtained by other groups. Our results do not agree very well with the analysis of experiment by Lee[5] and differ from his values by 60% in the ⟨110⟩ direction and by 28% in the ⟨100⟩ direction. The agreement with the work of Nowak[2] is better, with 10% and 28% agreement in the ⟨110⟩ and ⟨100⟩ directions, respectively. The values of $\lambda_{\vec{k}}$ calculated by Das[3] are also plotted in Fig. 1. We have very good agreement with the results of Schmidt and Mann,[4] who have used wave functions composed of both plane waves and Bloch sums of atomic $d$ functions and have used a pseudopotential to calculate the electron-phonon matrix elements. The results of Schmidt and Mann[4] plotted in Fig. 1 are the ones obtained by using the

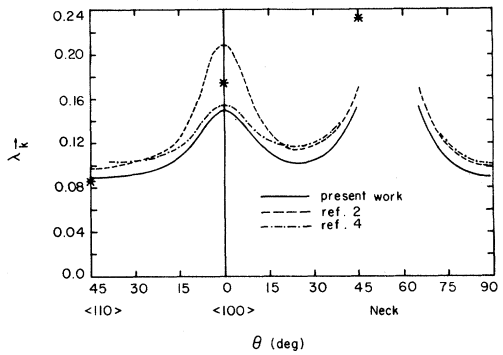


FIG. 1. Electronic mass enhancement $\lambda_{\vec{k}}$ of Cu for $\vec{k}$ lying on the (010) and (110) symmetry planes. The results of Das (Ref. 3) are given by the symbol *.

pseudopotential denoted by *CH* 2 in their paper. The contour plot of $\lambda_{\vec{k}}$ drawn on $\frac{1}{18}$th of the FS is shown in Fig. 3.

In a previous paper[10] we expanded $\lambda_{\vec{k}}$ in terms of different orthonormal polynomials on the FS, and found that the Fermi-surface harmonics (FSH) in $\vec{k}$ polynomials [FSH($\vec{k}$)] show good convergence. With the use of the results of Ref. 10, the following equation represents our $\lambda_{\vec{k}}$ to 2% accuracy:

$$\lambda_{\vec{k}}=-0.46476+1.4626k^2-0.8486k^4\,,$$

where $\vec{k}$ is measured in units of $2\pi/a$. If we include the next FSH, which gives an additional

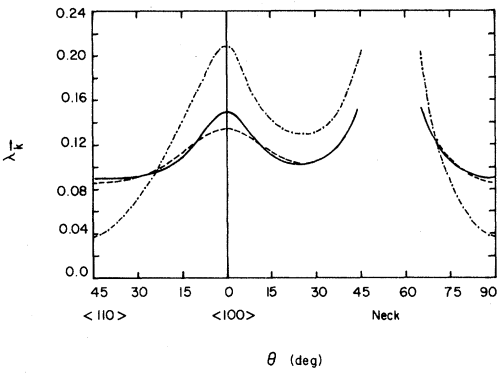


FIG. 2. Electronic mass enhancement $\lambda_{\vec{k}}$ of Cu for $\vec{k}$ lying on the (010) and (110) symmetry planes. Solid line gives our $\lambda_{\vec{k}}$. The dashed line is a fit to our results using Fermi surface harmonics (see text). The dash and dot line is the interpretation of experiment by Lee (Ref. 5).

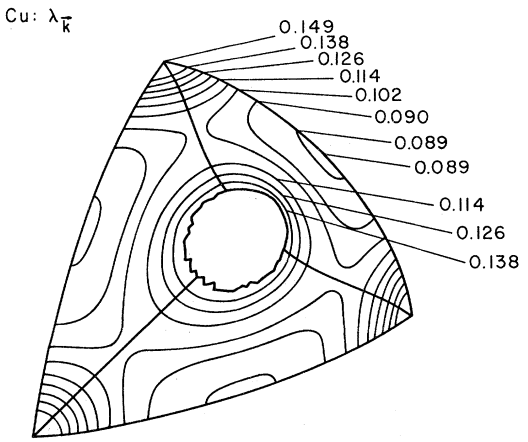


FIG. 3. Contours of constant $\lambda_{\vec{k}}$ shown on $\frac{1}{8}$th of the Fermi surface of Cu. The bold lines are intersections of the Fermi surface with the (100) and (110) planes, not contours. The jagged line is boundary of the neck on the face of the Brillouin zone in the ⟨111⟩ direction. The jaggedness reflects the finite mesh size. Because of the way we have chosen the spacing of sampling rays, the mesh is coarsest near the neck where there is a glancing angle of intersection.

term in the expansion of $\lambda_{\vec{k}}$ of the form $A(k_x^4+k_y^4+k_z^4)$, the convergence improves by only 0.05%.

## III. PHONON-LIMITED LIFETIMES

The quasiparticle lifetime is given by the expression [Ref. 1, Eq. (5.63)]

$$1/\tau(\vec{k},\omega)=2\pi\int_0^\infty d\Omega\,\alpha^2F(\vec{k},\Omega)\times[2N(\Omega)+f(\Omega+\omega)+f(\Omega-\omega)]\,, \tag{3}$$

$$\alpha^2F(\vec{k},\Omega)=\frac{1}{N}\sum_{\vec{k}'}\sum_{\nu}|g^{\nu}_{\vec{k},\vec{k}'}|^2\delta(\Omega-\omega^{\nu}_{\vec{k}-\vec{k}'})\times\delta(\epsilon_{\vec{k}'})\,. \tag{4}$$

For $\omega=0$ and $T\ll\omega_D$ ($\omega_D$ is the Debye energy), only small values of $\Omega$ contribute to the integral in (3). In this regime $\alpha^2F(\vec{k},\Omega)$ is quadratic in $\Omega$ and $1/\tau(\vec{k},0)$ varies as $T^3$ (Ref. 14):

$$\alpha^2F(\vec{k},\Omega)=\alpha_{\vec{k}}\Omega^2\quad(\Omega\ll\omega_D)\,, \tag{5}$$

$$1/\tau(\vec{k},0)=c_{\vec{k}}T^3\,,\qquad c_{\vec{k}}=14\pi\zeta(3)\alpha_{\vec{k}}\quad(T\ll\omega_D)\,, \tag{6}$$

where $\zeta(3)$ is the Riemann's zeta function [$\zeta(3)=1.202$] and Eq. (6) is obtained by using Eqs. (5) and (3). The experimental rate $1/\tau^*_{\vec{k}}$ differs from Eq. (6) in two ways.[14] First, at temperature $T$, electrons are sampled not just at the Fermi energy ($\omega=0$) but in a shell of thickness $T$. This can be approximately taken into account by averaging Eq. (6) by $-\partial f/\partial\omega$, which enhances $1/\tau_{\vec{k}}$ by $\frac{12}{7}$. Second, $1/\tau_{\vec{k}}$ is reduced by $1+\lambda_{\vec{k}}$, the mass-enhancement factor.

Calculation of $\alpha^2F(\vec{k},\Omega)$ needs the same ingredients as are needed for the calculation of $\lambda_{\vec{k}}$, and the construction of a histogram of $\alpha^2F(\vec{k},\Omega)$ proceeds in a similar fashion. The only difference in the procedure is that the $\Omega$ axis is divided into bins and as the vector $\vec{k}'$ traces the FS, contributions given by Eq. (4) are made to the appropriate $\Omega$ bin dictated by the delta function $\delta(\Omega-\omega^{\nu}_{\vec{k}-\vec{k}'})$. Results of $\alpha^2F(\vec{k},\Omega)$ for $\vec{k}$ lying along the ⟨110⟩, ⟨100⟩, and "neck" (⟨111⟩) directions are given in Fig. 4. It is obvious from the figure that it is difficult to determine the $\Omega^2$ behavior of $\alpha^2F(\vec{k},\Omega)$ for small $\Omega$ from these histograms. One way to over-

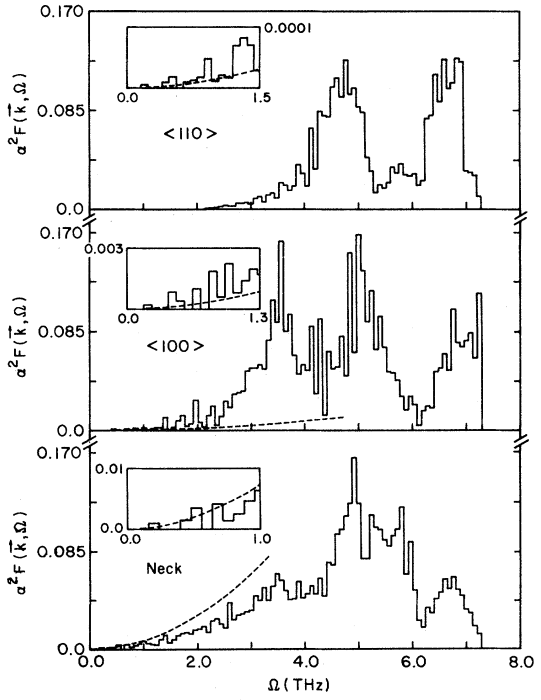


FIG. 4. Histograms of $\alpha^2F(\vec{k},\Omega)$ for $\vec{k}$ lying in the ⟨100⟩, ⟨110⟩, and "neck" (⟨10.065 1⟩) directions. The dashed line represents $\alpha_{\vec{k}}\Omega^2$ where $\alpha_{\vec{k}}=\alpha^2F(\vec{k},\Omega)/\Omega^2$ for small $\Omega$. The insets are enlarged views of the small-$\Omega$ region.

come this difficulty would be to increase the number of $Q$ bins in the BZ and to make the FS mesh finer, if needed, until the $\Omega^2$ behavior of $\alpha^2F(\vec{k},\Omega)$ for small $\Omega$ can be determined unambiguously from the histogram. This approach is extremely time consuming. Instead, we calculate the quadratic coefficient $\alpha_{\vec{k}}$ directly.

For small $\Omega$, the delta function $\delta(\Omega-\omega^{\nu}_{\vec{k}-\vec{k}'})$ in Eq. (4) restricts $\vec{k}'$ to lie near $\vec{k}$, i.e., the integration is over small values of $\vec{Q}$ where $\vec{Q}\equiv\vec{k}-\vec{k}'$. For small $Q$ the matrix element $\langle k \mid \nabla\vec{V} \mid \vec{k}+\vec{Q}\rangle$ is linear in $Q$ and therefore it can be replaced by $\vec{M}(\vec{k},\theta,\phi)Q$, where the angles $\theta$ and $\phi$ give the direction of the vector $\vec{Q}$. Similarly, $\omega^{\nu}_{Q}$ can be replaced by $v^{\nu}(\theta,\phi)Q$ in the small-$Q$ limit, where $v^{\nu}(\theta,\phi)$ is the sound velocity associated with the phonon of branch $\nu$ and the direction of propagation is given by $\theta$ and $\phi$. The delta function $\delta(\Omega-\omega^{\nu}_{\vec{Q}})$ in Eq. (4) can be used to perform the integration over $Q$. The remaining integral is over directions of $\vec{Q}$, where $\vec{Q}$ lies in a plane tangent to the FS at the point $\vec{k}$. Therefore, the integration in Eq. (4) is reduced to one dimension, which gives the following expression for $\alpha_{\vec{k}}$:

$$\alpha_{\vec{k}}=\frac{V}{(2\pi)^3}\frac{1}{2Mv_{\vec{k}}}\int_0^{2\pi}d\theta\sum_{\nu}\left|\frac{\hat{\epsilon}^{\nu}(\theta)\cdot\vec{M}(\vec{k},\theta)}{v^{\nu}(\theta)^2}\right|^2, \tag{7}$$

$$\vec{M}(\vec{k},\theta)\equiv\lim_{\vec{Q}\to 0}\frac{\langle\vec{k}\mid\nabla\vec{V}\mid\vec{k}+\vec{Q}\rangle}{\mid\vec{Q}\mid}. \tag{8}$$

The limit in (8) is to be taken such that $\vec{Q}$ lies in the plane tangent to the FS at $\vec{k}$ making an angle $\theta$ relative to a reference direction on the tangent plane.

Now the task is to evaluate $\vec{M}(\vec{k},\theta)$. This can be done by creating a sufficiently fine local mesh around each $\vec{k}$ point of interest. There is little guidance in earlier work to indicate how fine a mesh is needed for the limit (8) to be accurate. Therefore, we examined this question in detail and found that our existing mesh of 492 points was sufficient to get $\vec{M}(\vec{k},\theta)$ to about 5% accuracy provided some care was exercised. Figure 5 shows that $\vec{M}(\vec{k},\theta)$ is quite well specified simply by taking values of $\langle\vec{k}\mid\nabla\vec{V}\mid\vec{k}+\vec{Q}\rangle/\mid\vec{Q}\mid$ for $\mid\vec{Q}\mid$ $<0.1(2\pi/a)$ without explicitly taking the $Q\to 0$ limit. The fluctuations are not very large and are smoothed by doing the $\theta$ integral. The final calculations used typically 40 angles $\theta_i$, taking $M(k,\theta_i)$ to be defined by the smallest $\vec{Q}$ in the direction $\theta_i$ on our mesh, up to a maximum of $0.08\ (2\pi/a)$. Polarization vectors $\hat{\epsilon}^{\nu}(\theta)$ and sound velocities $v^{\nu}(\theta)$ were taken from experimental elastic constants.[15(a)] The function $V^{\nu}_{\theta}(\vec{k})$ $\equiv\hat{\epsilon}^{\nu}(\theta)\cdot\vec{M}(\vec{k},\theta)$ is quite anisotropic, especially for $\nu$

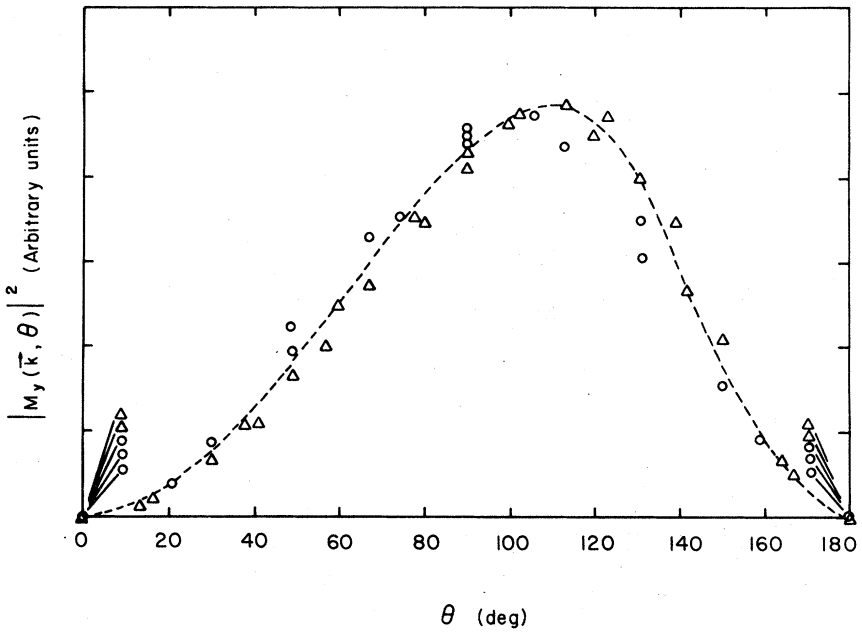


FIG. 5. Plot of $|M_y(\vec{k},\theta)|^2=|\langle\vec{k}\mid\nabla_y V\mid\vec{k}+\vec{Q}\rangle|^2/|\vec{Q}|^2$ as a function of $\theta$ for the $\vec{k}$ point (0.38,0.0,0.65). The angles $\theta=0$ and 180° correspond to $\vec{Q}$ in the plane $Q_y=0$ where this matrix element vanishes. Since the $\vec{k}$ point lies in a mirror plane, $-\theta$ is symmetric with $\theta$. The open circles represent points for which $|\vec{Q}|\leq 0.06(2\pi/a)$ and the triangles, points for which $0.06(2\pi/a)<|\vec{Q}|\leq 0.1(2\pi/a)$.

corresponding to transverse phonons.

The resulting values of $\alpha_{\vec{k}}\Omega^2$ are drawn in Fig. 4 along with the histograms of $\alpha^2F(\vec{k},\Omega)$ for three specific directions of $\vec{k}$. Also shown in Fig. 4 is an enlarged view of the small-$\Omega$ region from which we see that the histogram is consistent with $\alpha_{\vec{k}}\Omega^2$ for small $\Omega$. The crossover to more complicated behavior occurs somewhere in the range 5—10% of the maximum phonon frequency, $\omega_M$.

The temperature dependence of $1/\tau_{\vec{k}}$ goes as $T^3$ only at sufficiently low $T$. For a pure Debye spectrum, the $T^3$ law is fairly accurate up to $0.2\Theta_D$, but the departure of $\alpha^2F(\vec{k},\Omega)$ from Debye $\Omega^2$ behavior at fairly low $\Omega$ causes the $T^3$ regime to end at a much lower $T$, typically $0.02\Theta_D$. Specifically, we have examined this in detail by doing the integral in Eq. (3) for the three $\vec{k}$ points in the ⟨100⟩, ⟨110⟩, and "neck" directions. It is necessary to choose a crossover frequency $\Omega_c$, above which $\alpha^2F(\vec{k},\Omega)$ is given by the histogram in Fig. 4, and below which the limiting $\alpha_{\vec{k}}\Omega^2$ form is used. The results are given in Fig. 6. In each case the frequency $\Omega_c$ was varied by $\sim\pm40\%$ with no discernible change in the $1/\tau_{\vec{k}}$ curves. Above 4 K, the departure from $T^3$ becomes noticeable in all three cases.

The coefficient $c_{\vec{k}}$ ($1/\tau_{\vec{k}}=c_{\vec{k}}T^3$) in symmetry planes is shown in Fig. 7, along with experimental results and previous calculations by other groups. Selected values are also given in Table I for symmetry directions. Experimental values of $c_{\vec{k}}$ were measured by Doezema and Koch[6] (DK) using surface-Landau-level resonances at microwave frequencies. We have multiplied their values by $\frac{7}{12}$ and given them in Fig. 7 as open circles. We have not multiplied the results by $1+\lambda_{\vec{k}}$ since $\lambda_{\vec{k}}$ is small. The results of DK are higher than ours, specifically by a factor of 20 in the ⟨110⟩ direction, 5.4 in the ⟨100⟩ direction, and 1.15 in the "neck" direction. We attribute part of this difference to the fact that whereas our results suggest that $1/\tau_{\vec{k}}$ shows a $T^3$ behavior only up to about 4 K, the experimental values of $c_{\vec{k}}$ used data points obtained at much higher temperatures. DK (Ref. 6) determined the experimental values of $c_{\vec{k}}$ by plotting $1/\tau_{\vec{k}}$ vs $T^3$; their $c_{\vec{k}}$ is the slope of a straight line fitted to these points. For the "neck" and ⟨100⟩ directions, the data points to which the straight line is fitted are almost all at temperatures above 4 K extending up to 13 K, except for one or two points which lie in the 0 to 4 K range. The data points for determining $c_{\vec{k}}$ for the ⟨110⟩

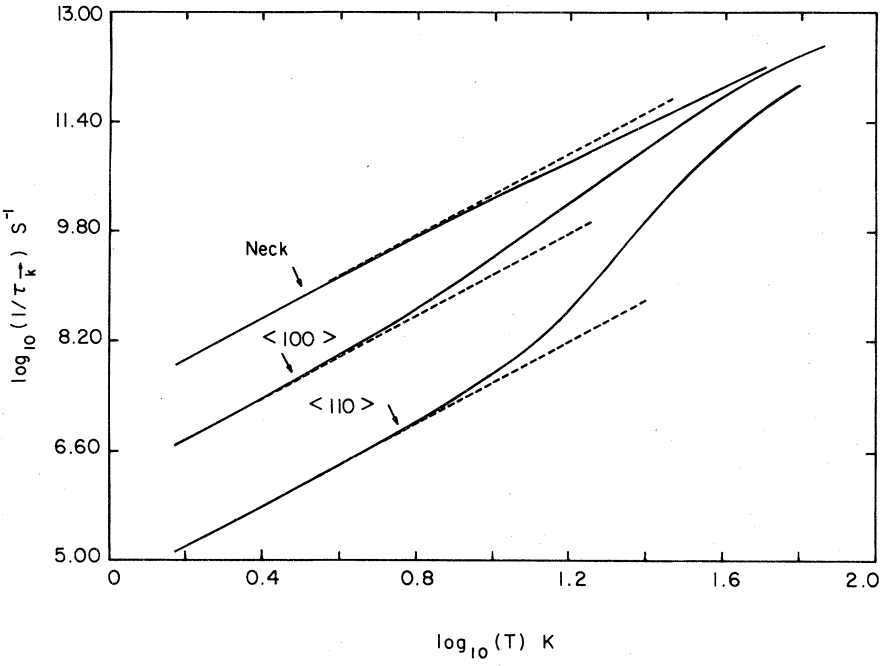


FIG. 6. Graphs of $\log_{10}(1/\tau_{\vec{k}})$ against $\log_{10}(T)$ for $\vec{k}$ lying in the ⟨110⟩, ⟨100⟩, and "neck" directions on the Fermi surface of Cu. The solid lines are the results obtained by using the histograms of $\alpha^2F(\vec{k},\Omega)$ given in Fig. 4 for $\Omega>\Omega_c$ and using the small-$\Omega$ form: $\alpha_{\vec{k}}\Omega^2$ for $\Omega<\Omega_c$. A value of 0.7 THz has been used for $\Omega_c$. The dashed line is obtained by using a Debye $\alpha^2F(\vec{k},\Omega)$.

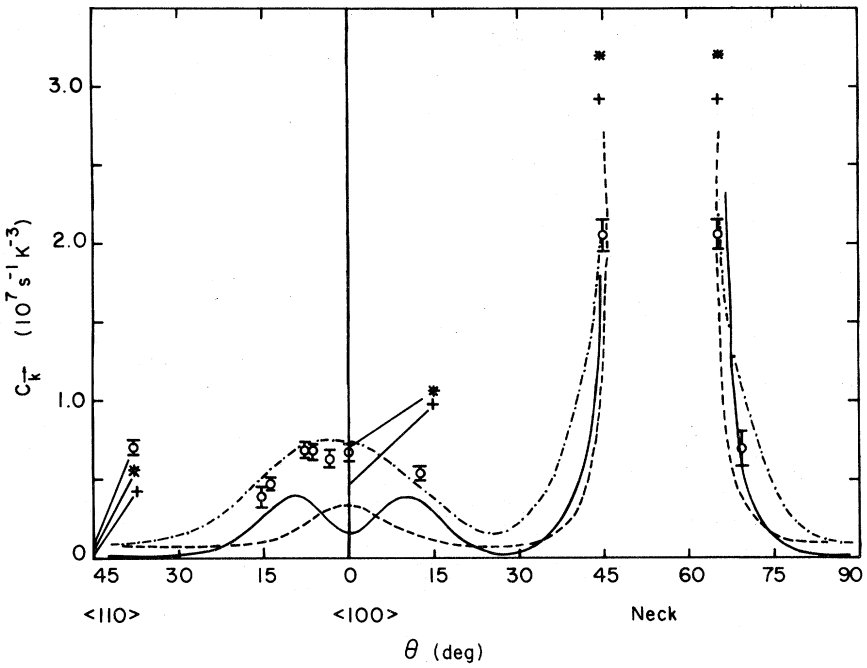


FIG. 7. Results of $c_{\vec{k}}=1/\tau_{\vec{k}}T^3$ $(T\to 0)$ for $\vec{k}$ lying in the (100) and (110) symmetry planes. Solid line is our results. The dashed line is the $c_{\vec{k}}$ calculated by Nowak (Ref. 2). The dash and dot line shows $1/\tau_{\vec{k}}T^3$ calculated by Schmidt and Mann (Ref. 4) for $T=12$ K with the use of their $CH2$ pseudopotential. The crosses are their results using Eq. (4) of Ref. 4 [Eq. (7) of this paper]. The results of Doezema and Koch (Ref. 6) are represented by open circles and the values found by Das (Ref. 3) by the symbol *.

direction have not been given in Ref. 6 but it is mentioned that temperatures in the neighborhood of 25 K were used to obtain $c_{\vec{k}}$ for this direction. In Fig. 8 we have plotted DK's values of $1/\tau_{\vec{k}}$ against $T^3$ for the "neck" and ⟨100⟩ directions. The residual scattering rate has been subtracted from $1/\tau_{\vec{k}}$ so that the values of $1/\tau_{\vec{k}}\to 0$ as $T\to 0$; $1/\tau_{\vec{k}}$ has also been multiplied by $\frac{7}{12}$. The solid line represents our calculated values of $1/\tau_{\vec{k}}$ and the dashed line is tangent to the solid line at $T=0$, i.e., the calculated $c_{\vec{k}}T^3$. In Fig. 9 we have plotted our calculated values of $1/\tau_{\vec{k}}$ vs $T^3$ for the ⟨110⟩ direction (solid line) in the temperature range from 20 K to about 25 K, which is the temperature region used by DK, the dashed line has the same meaning as in Fig. 8, and the dotted line has the slope of $c_{\vec{k}}$ found by DK. It is clear from Figs. 8 and 9 that our calculations agree well with the experimental data of DK for the ⟨110⟩ and the "neck" direction but not so well in the ⟨010⟩ direction, where our values of $1/\tau_{\vec{k}}$ lie about a factor of 2.5 below experiment. We have no explanation for this remaining discrepancy. There is a "dip" near the ⟨100⟩ direction in our calculated $c_{\vec{k}}$ which was not found by other authors. This seems to be a real feature of our calculation associated with wave-function character. The experimental results (which are especially reliable in this direction[15(b)] suggest that the dip is not real. Ap-

TABLE I. Values of $c_{\vec{k}}\equiv(1/\tau_{\vec{k}})T^{-3}$ found by different groups along the ⟨100⟩, ⟨110⟩, and "neck" (⟨111⟩) directions. The results of Schmidt and Mann (Ref. 4) are obtained by using Eq. (4) of Ref. 4 and have been taken directly from Fig. 1 of Ref. 4. Their value of $c_{\vec{k}}$ along the ⟨110⟩ direction is too small to be accurately read off from the figure and is not given in this table. Results of Refs. 2–4 and 6 have been multiplied by a factor of $\frac{7}{12}$.

| | $c_{\vec{k}}=(1/\tau_{\vec{k}})T^{-3}$ ($10^7$ $s^{-1}K^{-3}$) | | |
|---|---|---|---|
| | ⟨100⟩ | ⟨110⟩ | "Neck" |
| Present work | 0.149 | 0.004 | 2.18 |
| Schmidt & Mann[a] | 0.5 | | 2.9 |
| Nowak[b] | 0.34 | 0.07 | 2.8 |
| Das[c] | 0.70 | 0.07 | 3.2 |
| Doezema and Koch[d] | 0.81 | 0.08 | 2.52 |

[a]Reference 4.
[b]Reference 2.
[c]Reference 3.
[d]Reference 6.

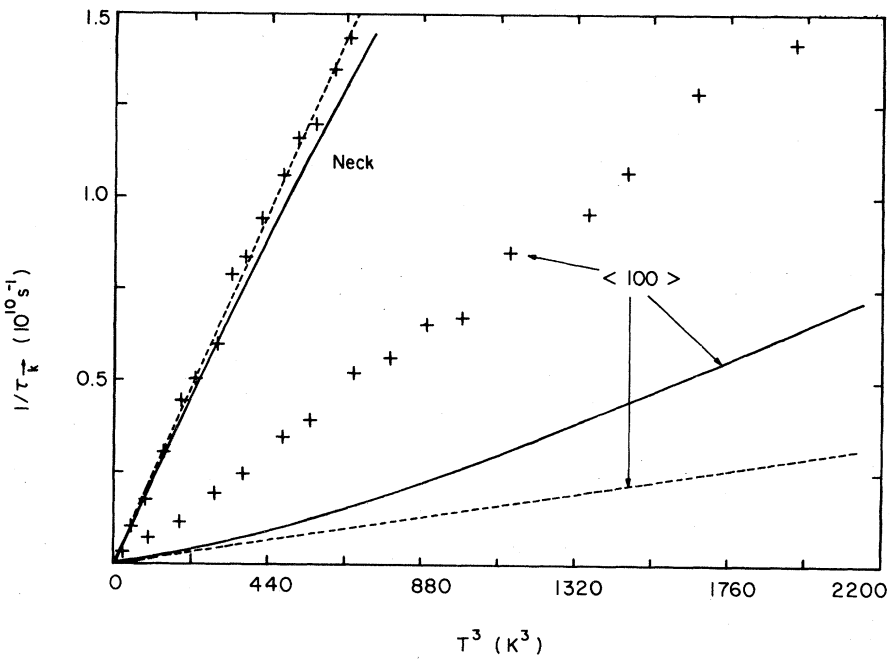


FIG. 8. Experimental results of $1/\tau_{\vec{k}}$ obtained by Doezema and Koch (taken from Fig. 4 of Ref. 6) for the ⟨100⟩ and "neck" directions are represented by the symbol +. The solid line and the dashed line are our results of $1/\tau_{\vec{k}}$ and are the same as the solid and dashed lines of Fig. 6 for the "neck" and ⟨100⟩ directions.

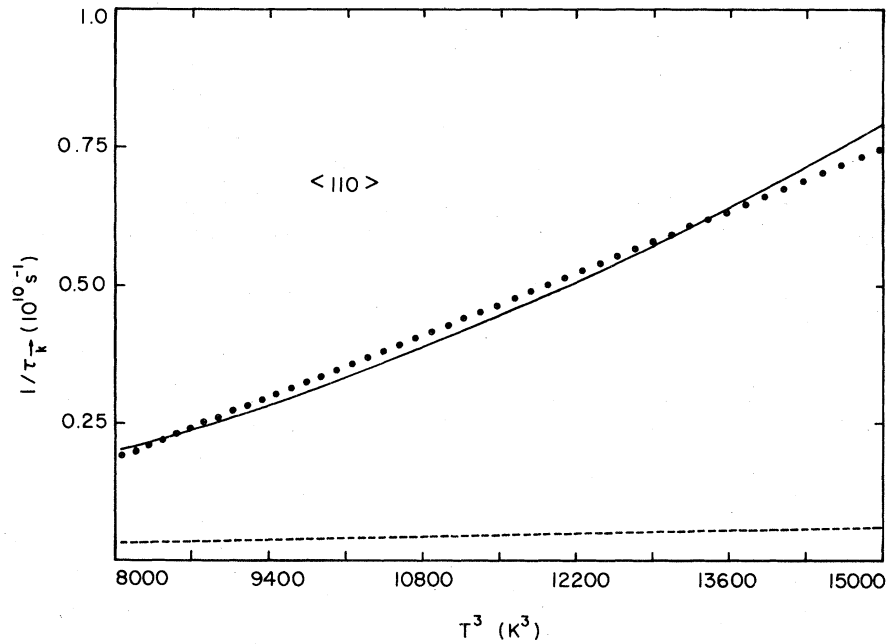


FIG. 9. Experimental results of $1/\tau_{\vec{k}}$ obtained by Doezema and Koch (Ref. 6) for the ⟨110⟩ direction. The dotted line is a straight line with slope equal to the $c_{\vec{k}}$ found by Doezema and Koch ($c_{\vec{k}} = 1/\tau_{\vec{k}} T^3$). The solid line and the dashed line are our results and are the same as the solid and dashed lines of Fig. 6 in the ⟨110⟩ direction.

parently the experimental values of $c_{\vec{k}}$ do not represent the true low-$T$ limit because extrapolation to $T=0$ can not be performed safely unless data below 4 K are available. Thus the "data" in Fig. 7 should not be compared closely with theory. This is consistent with conclusions of Schmidt and Mann[4] (SM). Therefore, when comparing with experiment, SM plotted $1/\tau_{\vec{k}}T^3$ calculated at 12 K instead of its low-$T$ limit, $c_{\vec{k}}$. This is what is given in Fig. 7 as the dash-dot line. The points represented by the symbol + are the values of $c_{\vec{k}}$ obtained by SM using Eq. (7) [Eq. (4) of Ref. 4] and lie much lower than the experimental values of DK (except for the "neck" direction).

Nowak[2] used methods somewhat similar to ours, and his values of $c_{\vec{k}}$ are plotted in Fig. 7 (the dashed curve). Nowak assumed that only longitudinal phonons contribute in Eq. (7) for the belly region. He also set the longitudinal-sound velocity $v^L(\theta)$ in Eq. (7) equal to a constant $4.69\times10^5$ cm sec$^{-1}$, for $\vec{k}$ lying on the belly. Our results show that even for $\vec{k}$ points on the belly, transverse phonons make an appreciable contribution to $1/\tau_{\vec{k}}$, e.g., for the $\langle 100\rangle$ direction the contributions are 45% and 55% from the longitudinal and transverse phonons, respectively. Also we find that the longitudinal-sound velocity $v^L(\theta)$ varies with $\theta$ (from 5 to 4.4 for the $\langle 100\rangle$ direction and from 5.2 to 4.4 for the $\langle 110\rangle$ direction in units of $10^5$ cm sec$^{-1}$). Nowak has not made these approximations for the neck region, where his results match very well with ours. The results of Das[3] are shown by the symbol * in Fig. 7. Note that the results of Nowak, Das, SM, and DK have all been multiplied by the factor $\frac{7}{12}$ to compare with our results obtained by Eq. (7). There is apparently a factor of $\frac{7}{8}$ error in the equations for $1/\tau_{\vec{k}}$ (at low $T$) used by both Nowak and Das. We have not corrected for this in plotting their results. The contour of $c_{\vec{k}}$ drawn on $\frac{1}{8}$th of the FS is shown in Fig. 10.

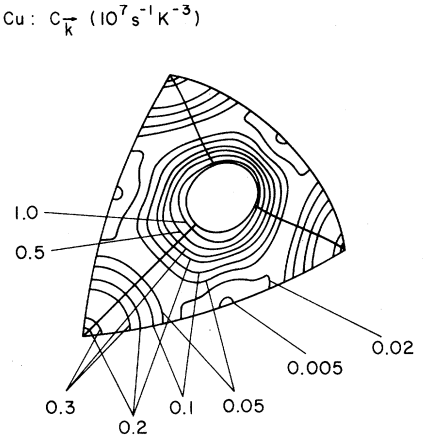


FIG. 10. Contours of constant $c_{\vec{k}}=1/\tau_{\vec{k}}T^3$ ($T\to0$) drawn on $\frac{1}{8}$th of the Fermi surface of Cu. (See the caption of Fig. 3.)

## IV. CONCLUSION

Although our values of $\lambda_{\vec{k}}$ do not match extremely well with the interpretation of experiment by Lee[5] (Fig. 2), it should be kept in mind that for the interpretation of experiment band-structure values of electronic velocities $v_{\vec{k}}$ are needed. A value of $1+\lambda_{\vec{k}}$ is obtained by comparing measured and calculated velocities. Because $\lambda_{\vec{k}}$ is only of order 0.1, a 10% uncertainty in the band velocity becomes a 100% uncertainty in $\lambda_{\vec{k}}$. We suggest that our results are not necessarily inconsistent with experiment. Similarly our values of $c_{\vec{k}}=(\tau_{\vec{k}}T^3)^{-1}$ disagree with experiment, but the experiment actually did not achieve the true low-temperature limit of $1/\tau_{\vec{k}}T^3$. In those cases where a direct comparison was made (Figs. 8 and 9), very good agreement was found for the $\langle 110\rangle$ and "neck" direction and a difference of about a factor of 2 in the $\langle 010\rangle$ direction.

We get a value of 0.11 for $\lambda$ (the average of $\lambda_{\vec{k}}$ over the FS). This agrees well with earlier calculations.[2-4] It also agrees reasonably with experimental values of $\lambda$ inferred from superconductivity. Hoyt and Mota[16] have estimated $\lambda$ for pure Cu by extrapolating values of $\lambda$ obtained from the McMillan[17] equation, for superconducting Cu-Ga alloys. They find $\lambda=0.16$. Chaikin[18] *et al.* have used proximity tunneling measurements to extract a value of $\lambda=0.10\pm0.02$ for pure Cu.

The only uncontrolled aspect of our calculation is the RMT model. The results of this paper and the next paper[11] increase our confidence in the RMT model. Earlier work[19] suggested that the RMT model worked badly at long wavelengths for Nb. In contrast, we find that the present version of the RMT model works quite nicely at long wavelengths for Cu. It is encouraging to note that although SM (Ref. 4) have used a very different method without the use of the RMT model, their results agree well with our calculation. Expansion of $1/\tau_{\vec{k}}$ in terms of FSH($v_{\vec{k}}$) and FSH($\vec{k}$) gives a convergence of only 8% and 10% accuracy, respectively, even when 16 orthogonal polynomials are used.

## ACKNOWLEDGMENTS

We thank T. P. Beaulac and B. Mitrović for help. Work at Stony Brook was supported in part by NSF Grant No. DMR79-00837. Work at Oak Ridge was sponsored by the Division of Materials Sciences, U.S. Department of Energy under Contract No. W-7405-eng-26 with the Union Carbide Corporation.

## APPENDIX: ADJUSTED RIGID MUFFIN-TIN APPROXIMATION FOR THE ELECTRON-PHONON INTERACTION IN NOBLE AND SIMPLE METALS

In order to calculate the electron-phonon matrix elements, one needs to know the self-consistent change in crystal potential $\delta V(r)$ which results from an infinitesimal displacement of one of the atoms $\delta R_n$. The rigid muffin-tin approximation[20,21] consists of approximating this change by

$$\frac{\delta V(r)}{\delta R}=\begin{cases}-\nabla_\alpha V(r), & r \in \text{cell } n \\ 0 \text{ otherwise}, & \end{cases} \tag{A1}$$

where $V(r)$ is the total crystal potential. The name "rigid muffin-tin" is attached to this approximation because $V(r)$ is usually approximated by a sum of nonoverlapping, spherical potentials (muffin-tins)

$$V(r)=\sum_n v_{\mathrm{MT}}(r-R_n)-V_0 \ . \tag{A2}$$

Equation (A1) is equivalent to moving one of these muffin-tins rigidly when an atom is displaced.

The rigid muffin-tin approximation gives reasonably accurate results for the average magnitude of the electron-phonon matrix elements in transition metals.[19,22] This is probably because the largest contributions to the matrix elements involve $d$ electrons which (we expect) move relatively rigidly with the atom. Equation (A1) is, however, not appropriate for the simple metals. In the limit of a weakly perturbed electron gas, there is an accepted procedure for calculating the electron-phonon matrix elements.[23,24] In this case, the crystal potential is written as a sum of screened ionic potentials $v_{\mathrm{sc}}(r)$ which move rigidly when an atom is displaced:

$$V(r)=\sum_n v_{\mathrm{sc}}(r-R_n) \ , \tag{A3}$$

$$\frac{\delta V(r)}{\delta R_{n\alpha}}=-\nabla_\alpha v_{\mathrm{sc}}(r-R_n) \ . \tag{A4}$$

For calculating the energy bands, the two forms for the crystal potential are equivalent. They differ, however, for the electron-phonon interaction. The rigid muffin-tin approximation significantly underestimates the strength of the electron-phonon coupling in the limit of weak scattering. The reason for this is that the two types of potentials correspond to two different ways of apportioning the same total crystal potential among the ions.[25,26] The muffin-tin potentials vanish for $r$ greater than $r_{\mathrm{MT}}$, the radius of the largest sphere that will fit entirely within a Wigner-Seitz cell, and their values are referenced to the muffin-tin zero (the average value of the interstitial potential). The screened ionic potentials have a longer range (their tails overlap) and their values are referenced to the vacuum as zero.

For a noble metal such as Cu, neither the rigid muffin-tin approximation nor the simple linear-screening theory is rigorously applicable. Nevertheless, we have made an *ad hoc* adjustment to the rigid muffin-tin approximation which improves the agreement with experiment and (we believe) with reality. Similar adjustments have been made before.[2,27,28] The rigid muffin-tin potential can be made stronger and it can be given a longer range without affecting the electronic structure by simply adding to it a potential which is constant throughout its Wigner-Seitz cell:

$$v_{\mathrm{WS}}(r-R_n)=v_{\mathrm{MT}}(r-R_n)+\theta_n(r)v_0 \ , \tag{A5}$$

$$\theta_n(r)=\begin{cases}1, & r \in \text{cell } n \\ 0 \text{ otherwise} \ . & \end{cases} \tag{A6}$$

This maneuver only affects the band structure by causing a rigid shift equal to $v_0$.

One problem with a potential such as that of Eq. (A5) is that the KKR method is no longer rigorously applicable. This is not a serious practical problem for fcc metals, however. If one calculates the phase shifts for scattering off of a spherically ized version of Eq. (A5) and plugs them into the KKR equation, keeping $v_0$ on the order of 0.5 Ry or less, one obtains essentially the same band structure as for $v_0$ equal to zero.[29] The insensitivity of the KKR band structure to $v_0$ is equivalent to the empirical result that when Fermi surface data are fitted using a KKR phase-shift parametrization, good fits are obtained for a wide range of values of the energy parameter. Figure 11 shows phase shifts calculated for Cu using a spherically ized form of (A5) [$\theta_0(r)=1$, $r<r_{\mathrm{WS}}$] and a range of values of $v_0$. Also shown for comparison are phase shifts fitted empirically to de Haas–van Alphen data.[2,30] The shifted potentials give at least as good a Fermi

surface as the original muffin-tin potential.

In order to complete the prescription for the adjusted potential, we must specify the magnitude of the shift $v_0$. We attempted to choose $v_0$ so that $v_{WS}(r)$ satisfied the following result which is valid for a weak ionic potential in a electron gas, linearly screened[31,32]:

$$\frac{1}{\Omega_a}\int_0^\infty v_{sc}(r)r^2dr=-Z/N(E_F)\ , \tag{A7}$$

where $\alpha_a$ is the volume per atom and $N(E_F)$ is the Fermi-energy density of states (both spins). When Eq. (A7) is applied to a real metal, $v_{sc}(r)$ must be interpreted as a screened pseudopotential and $Z$ as the number of valence electrons. Linear screening suggests this result is valid for $Z \ll 1$.

Since our formula for rigid muffin-tin electron-phonon matrix elements is written in terms of the Fermi-energy phase shifts, we need to write Eq. (A7) in terms of phase shifts. This is easily accomplished by expanding the Fourier transform of $v_{sc}(r)$ in terms of spherical harmonics:

$$\begin{aligned}\hat{v}_{sc}(q)&=\int_0^\infty \exp[i(k-k')r]v_{sc}(r)d^3r/\Omega_a\\&=\frac{4\pi}{\Omega_a}\sum_l(2l+1)P_l(\hat{k}\cdot\hat{k}')\\&\quad\times\int_0^\infty r^2dr\,j_l(kr)j_l(k'r)v_{sc}(r)\ ,\end{aligned} \tag{A8}$$

where $q=k-k'$. Since we are interested only in scattering between points $k$ and $k'$ which are on the Fermi surface, we can write Eq. (A8) in terms of the Fermi-energy phase shifts by using the approximation (valid for weak pseudopotentials),

$$\delta_l(E_F)\sim -k_F\int_0^\infty r^2dr\,j_l^2(k_Fr)v_{sc}(r)\ . \tag{A9}$$

Thus, Eq. (A7) may be written

$$\begin{aligned}\lim_{q\to 0}\hat{v}_{sc}(q)&\sim\frac{4\pi}{\Omega_a\sqrt{E_F}}\sum_l(2l+1)\delta_l(E_F)\\&=-Z/N(E_F)\ .\end{aligned} \tag{A10}$$

We adjusted $v_0$ so that the phase shifts from the potential $v_{WS}(r)$ satisfied (A10). The magnitude of the shift $v_0$ was 0.2825 Ry. The original and adjusted phase shifts are denoted by $A$ and $B$, respectively, in Fig. 11.

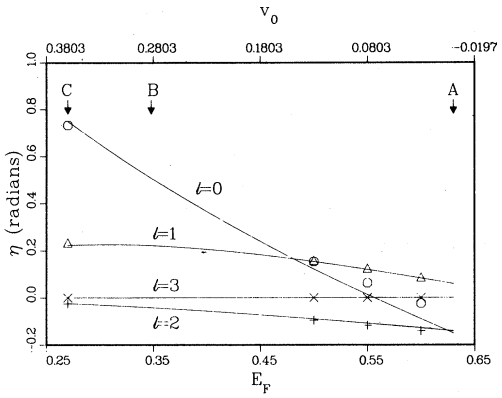


FIG. 11. Phase shifts for Cu using a sphericalized form of the potential given by Eq. (A5) (solid line). Phase shifts fitted empirically to de Haas–van Alphen data are also shown for comparison. The value of the Fermi energy used here is shown by $B$. See the text for an explanation of the other symbols used in the figure.

There are other ways of choosing $v_0$ which are equivalent to (A10) in the weak-scattering limit but which differ somewhat when applied to Cu. Nowak[2] chose a shift that set the Fermi surface average of the $q=0$ limit of the augmented plane wave form factor equal to $-Z/N(E_F)$. His choice is denoted by $C$ on the figure. Coleridge[28] proposed setting $E_F-E_{F0}=-Z/N(E_F)$ where $E_{F0}$ is the Fermi energy for free electrons, $E_{F0}=(3Z\pi^2/\Omega_a)^{2/3}$. This choice leads to phase shifts appropriate to an $E_F$ of 0.24. One could also argue in favor of satisfying the Friedel sum rule,

$$(2/\pi)\sum_l(2l+1)\delta_l(E_F)=Z\ .$$

This choice would lead to an even smaller value for $E_F$. We doubt that the differences between these proposals merit extended discussion. Self-consistent density-functional theory should be applied to this problem instead. This has not been done yet because of technical difficulties.

[1]G. Grimvall, in *Selected Topics in Solid State Physics*, edited by E. P. Wohlfarth (Elsevier, New York, 1981), Vol. XVI.
[2]D. Nowak, Phys. Rev. B 6, 3691 (1972).
[3]S. G. Das, Phys. Rev. B 7, 2238 (1973).
[4]H. Schmidt, and E. Mann, Phys. Status Solidi B 94, 95 (1979).
[5]M. J. G. Lee, Phys. Rev. B 2, 250 (1970).
[6]R. E. Doezema and J. F. Koch, Phys. Rev. B 6, 2071 (1972).

[7]W. H. Butler, J. J. Olson, J. S. Faulkner, and B. L. Gyorffy, Phys. Rev. B 14, 3823 (1976).
[8]W. H. Butler, F. J. Pinski, and P. B. Allen, Phys. Rev. B 19, 3708 (1979).
[9]F. S. Khan, P. B. Allen, and W. H. Butler, Physica B + C 108, 893 (1981).
[10]F. S. Khan and P. B. Allen, Phys. Status Solidi B 100, 227 (1980).
[11]T. P. Beaulac, P. B. Allen, and F. J. Pinski, Phys. Rev. B 26, 1549 (1982).
[12]R. M. Nicklow, G. Gilat, H. G. Smith, L. J. Raubenheimer, and M. K. Wilkinson, Phys. Rev. 164, 922 (1967).
[13]J. C. Shaw, J. B. Ketterson, and L. R. Windmiller, Phys. Rev. B 5, 3894 (1972).
[14]D. K. Wagner and R. Bowers, Adv. Phys. 27, 651 (1978).
[15](a) W. C. Overton and J. Gaffney, Phys. Rev. 98, 969 (1955); (b) R. E. Doezema (private communication).
[16]R. F. Hoyt and A. C. Mota, Solid State Commun. 18, 139 (1976).
[17]W. L. McMillan, Phys. Rev. 167, 331 (1968).
[18]P. M. Chaikin, G. Arnold, and P. K. Hansama, J. Low Temp. Phys. 26, 229 (1977).
[19]W. H. Butler, in *Physics of Transition Metals 1980,* edited by P. Rhodes (Institute of Physics, London, 1981), p. 505.
[20]N. F. Mott and H. Jones, *The Theory of the Properties of Metals and Alloys* (Dover, New York, 1936), p. 253.
[21]G. D. Gaspari and B. L. Gyorffy, Phys. Rev. Lett. 28, 801 (1972).
[22]W. H. Butler, in *Superconductivity in d- and f-Band Metals,* edited by H. Suhl and M. B. Maple (Academic, New York, 1980), p. 443.
[23]J. Bardeen, Phys. Rev. 52, 688 (1937).
[24]D. J. Scalapino, in *Superconductivity,* edited by R. D. Parks (Dekker, New York, 1969), p. 455.
[25]M. J. G. Lee and V. Heine, Phys. Rev. B 5, 3839 (1971).
[26]P. B. Allen and M. J. G. Lee, Phys. Rev. B 5, 3848 (1972).
[27]D. A. Papaconstantopoulos, A. D. Zdetisis, and E. N. Economou, Solid State Commun. 27, 1189 (1978).
[28]P. T. Coleridge, Phys. Rev. B 23, 3691 (1981).
[29]This fact forms the basis for several linearized KKR schemes, e.g., O. K. Andersen and R. V. Kasowski, Phys. Rev. B 4, 1064 (1971); J. S. Faulkner, *ibid.* 19, 6186 (1979).
[30]D. Nowak and M. J. G. Lee, Phys. Rev. B 5, 2851 (1972).
[31]V. Heine, P. Nozières, and J. W. Wilkins, Philos. Mag. 13, 741 (1966).
[32]J. M. Luttinger and P. Nozières, Phys. Rev. 127, 1423 (1962); 127, 1431 (1962).